Thermal Desorption Spectroscopy Evaluation of the Hydrogen-Trapping Capacity of NbC and NbN Precipitates

ELIEN WALLAERT, TOM DEPOVER, MUHAMMAD ARAFIN, and KIM VERBEKEN

In the current study, ferritic steels containing NbC or NbN precipitates were investigated. The materials were subjected to various heat treatments, giving rise to different precipitate size distributions as determined by transmission electron microscopy. Both NbC and NbN precipitates act as hydrogen traps. The steels were hydrogen charged both electrochemically and/or from the gaseous hydrogen source, followed by multiple thermal desorption spectroscopy (TDS) measurements. Electrochemical charging gave rise to a low-temperature peak [323 K to 523 K (50 °C to 250 °C)], originating from the hydrogen trapped near grain boundaries, with activation energy ranging between 24 and 33 kJ/mol, and at small NbC (39 to 48 kJ/mol) or NbN precipitates (23 to 24 kJ/mol). Gaseous charging caused a high-temperature TDS peak [723 K to 923 K (450 °C to 650 °C)], which was attributed to the presence of incoherent precipitates. The activation energy for NbC precipitates, charged in a hydrogen atmosphere, ranged between 63 and 68 kJ/mol and between 100 and 143 kJ/mol for NbN precipitates.

I. INTRODUCTION

ALTHOUGH the first detrimental effects of hydrogen on the mechanical properties of iron and steels were described by Johnson in 1875, many features of the involved mechanisms are still poorly understood and are the subject of debate. As a result of the rising demand for high-strength steels, since these materials are known to be sensitive to the harmful consequences of hydrogen, an increasing interest for hydrogen embrittlement research arose.

The introduction of nanocarbides or nanonitrides as hydrogen-trapping sites in steels is often discussed to play a crucial role in hydrogen embrittlement[1,2]. Carbides, such as VC, TiC, and NbC, are most often considered as hydrogen-trapping sites.

Asahi et al.[3] investigated hydrogen interaction with VC precipitates using thermal desorption spectroscopy (TDS) and estimated the activation energy for the de-trapping to be in the range of 33-35 kJ/mol. The trapping of hydrogen was also observed for this type of precipitates using small-angle neutron scattering (SANS) by Malard et al.[4] They concluded that the intensity increase was consistent with hydrogen being homogeneously distributed in the VC precipitate rather than at the precipitate/matrix interface. By cathodically charging austenitic Fe-Mn-C TWIP steel, 5 ppm wt pct H was mentioned to be trapped inside the VC precipitates.

TiC precipitates were investigated by Asaoka et al.[5] in a Fe-0.5 wt pct Ti alloy charged with tritium using an auto-radiographic method for observation. The binding energy was found to be above 61 kJ/mol. Pressouyre and Bernstein[6], however, found a trapping activation energy of 95 kJ/mol by means of the hydrogen permeation technique.[7] They also concluded that coherent TiC precipitates were not as effective traps as incoherent precipitates and that the activation energy increased with precipitate size. Lee and Lee[8] used TDS to determine the hydrogen interaction with the matrix–particle interface. They obtained an activation energy of 86.9 kJ/mol and a binding energy of 28.1 kJ/mol. With the same technique, Wei et al.[9] determined an activation energy of 85.7 kJ/mol for H desorption from incoherent TiC particles formed in a 0.05C-0.22Ti-2.0Ni alloy. While for another steel (0.42C-0.30Ti) in which larger incoherent Ti precipitates were formed, the activation energy was found to be 116 kJ/mol, the coherent particles had an activation energy of 46 to 59 kJ/mol. Pérez Escobar et al.[10] investigated TiC precipitates in an experimental steel (0.025 wt pct C-0.09 wt pct Ti), which was annealed in a hydrogen environment and electrochemically charged. TDS measurements showed two peaks, a low-temperature peak from the reversible traps, such as grain boundaries, and a high-temperature peak from the irreversible trapping by TiC precipitates. Wei and Tsuzaki[11] confirmed that hydrogen could not be trapped through cathodic charging at incoherent TiC precipitates, but heat treatment at high temperature [T = 1223 K (950 °C)] is required. The amount of trapped hydrogen depended on the precipitate volume and not on the particle/matrix interfacial area, which suggests that hydrogen was trapped inside the precipitates. Takahashi et al.[12] showed that hydrogen was trapped at the interface of the precipitate/matrix for small coherent precipitates by performing atomic-scale

ELIEN WALLAERT and TOM DEPOVER, Ph.D. Researchers, and KIM VERBEKEN, Professor, are with the Department of Materials Science and Engineering, Ghent University (UGent), Technologiepark 903, 9052 Ghent, Belgium. Contact e-mail: kim.verbeken@ugent.be MUHAMMAD ARAFIN, Research Engineer, is with the ArcelorMittal Global R&D Gent, OCAS NV, Technologiepark 935, 9052 Zwijnaarde, Belgium.
Manuscript submitted September 6, 2013.
Article published online January 10, 2014.

observation of deuterium atoms at the surfaces of nanosized TiC, using atom probe tomography.

Tsuzaki and co-workers[13] observed the presence of hydrogen near semicoherent NbC precipitates, having a disk shape with 5-nm length and 2-nm thickness, in a 0.97Fe-0.23C-0.25Nb-1.90Ni (in at. pct) steel after electrochemical charging using SANS. The hydrogen appeared to be trapped both inside the precipitate and at the precipitate–matrix interface. The NbC precipitates in a tempered martensite matrix showed a maximum hydrogen content when the material was tempered at 873 K (600 °C).[14] This was attributed to precipitate coarsening at higher temperatures. Hydrogen is considered to be trapped at the precipitate–matrix interface, especially at misfit dislocations. In their study, NbC precipitates are considered to consist of several hydrogen-trapping sites with variable activation energies, such as the precipitate–ferrite interface, the coherency strain region surrounding the precipitate (misfit dislocations), and the crystallographic defects inside the precipitate. The hydrogen-trapping capacity is argued to be higher than those for TiC and VC precipitates. However, their TDS spectra always consisted of low-temperature peaks [373 K to 623 K (100 °C to 350 °C)], indicating that, with the used cathodic hydrogen-charging methods, no hydrogen was irreversibly bound to NbC precipitates.[15]

In the current study, two alloys with Nb-containing precipitates in a ferritic matrix were processed and investigated. The samples were subjected to different heat treatments, giving rise to different precipitate size distributions as determined by transmission electron microscopy (TEM) analysis. The NbC or NbN precipitates were hydrogen charged electrochemically and/or from gaseous H_2, followed by multiple TDS measurements to investigate their hydrogen-trapping capacity.

II. EXPERIMENTAL PROCEDURE

The compositions of the used lab-cast materials, C080 and C081, are given in Table I and were chosen for stoichiometric reasons to promote the formation of NbC and NbN precipitates, respectively. These materials were produced in a Pfeiffer VSG100 vacuum melt and cast unit, operated under a protective argon gas atmosphere. The cast blocks had an initial thickness of 400 mm and after reheating at 1523 K (1250 °C) for 90 minutes, they were hot rolled. Hot rolling was performed in five steps: the first four with a reduction of 30 pct, and the last one with a reduction of 25 pct at 1273 K (1000 °C). After this, cold rolling with a reduction of 76 pct was applied, to reach at a final thickness of 1.7 mm.

In order to promote the formation of different precipitate size distributions, the materials were subjected to different heat treatments, as summarized in Table II. The heat-treatment conditions were based on thermodynamic calculations using Modips software, shown in Figure 1. Modips is a noncommercial software consisting of a database of precipitate solubility products based on the literature data. Two materials, C080-HT1 and C080-HT2, were treated in air at 1473 K (1200 °C) for 30 minutes and subsequently at 1073 K (800 °C) for 10 and 120 minutes, respectively, followed by air cooling to room temperature. The third material, C080-H_2, was heat treated in a H_2 atmosphere at 1073 K (800 °C) for 58 hours. The C081-HT material was treated in air at 1473 K (1200 °C) for 30 minutes and at 1173 K (900 °C) for 30 minutes, also followed by air cooling to room temperature. The fifth material C081-H_2 was heat treated under H_2 atmosphere at 1173 K (900 °C) for 39 hours and at 868 K (595 °C) for 12.5 hours. The use of long annealing duration for the materials that are treated in a H_2 atmosphere was necessary to reach equilibrium conditions in the samples. After the heat treatments, disk-shaped samples with a diameter of 20 mm were taken from the sheet and ground to a thickness of 1 mm.

For optical microscopy, the samples were ground and polished to 1 μm. Afterward, they were etched with a 2 pct nital solution and washed with methanol and acetone.

In order to verify the presence of NbC or NbN precipitates in the steel matrix, scanning transmission electron microscopy (STEM) analysis, using a JEM-2200FS, as well as energy dispersive X-ray (EDX) spectroscopy was performed. The thin foil samples were prepared by grinding and polishing the samples to a thickness below 100 μm. Afterward, the thin foil samples were electropolished, using a TenuPol-5 electropolishing unit of Struers, in a 10 pct perchloric acid and 90 pct acetic acid solution.

Two different hydrogen-charging methods were performed in the current study. The cathodic charging was performed for 1 hour, using a 0.5 M sulfuric acid

Table II. Summary of the Heat Treatments Performed on the Different Materials

Material	Heat treatment	Atmosphere
C080-HT1	30 min at 1473 K (1200 °C) 10 min at 1073 K (800 °C)	air
C080-HT2	30 min at 1473 K (1200 °C) 120 min at 1073 K (800 °C)	air
C080-H_2	58 h at 1073 K (800 °C)	H_2
C081-HT	30 min at 1473 K (1200 °C) 30 min at 1173 K (900 °C)	air
C081-H_2	39 h at 1173 K (900 °C) 12.5 h at 868 K (595 °C)	H_2

Table I. Chemical Compositions of the Materials Used (Weight Percent)

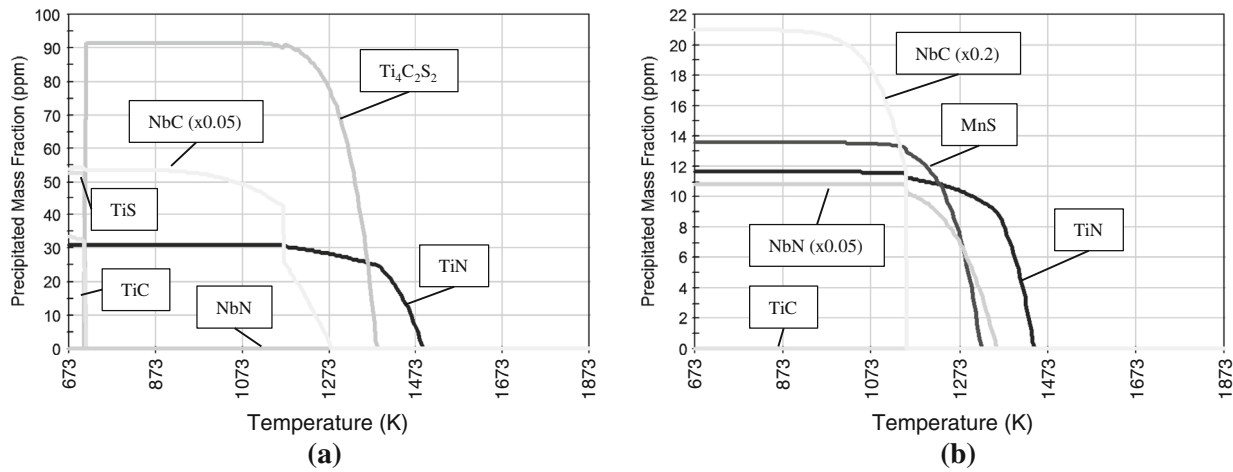|	C	Mn	Si	Nb	Ti	N	Others
C080 (Nb + C)	0.013	0.0049	0.0054	0.1	0.0092	0.0007	P, S, Al
C081 (Nb + N)	0.0012	0.21	0.0049	0.11	0.0009	0.0031	P, S, Al

Fig. 1—Modips calculations for the C080 (*a*) and C081 (*b*) materials.

aqueous solution containing 1 g/L thiourea, with a current density of 0.8 mA/cm^2 and a Pt counter electrode. These parameters are based on the results of a previous study.[16] Another method to introduce hydrogen into the samples was by performing gaseous charging during a heat treatment in the H$_2$ atmosphere. This charging procedure already demonstrated its hydrogen-charging effectiveness for TiC precipitates as was shown by Pérez Escobar *et al.*[17] The heat treatment was performed in a Nabertherm tube furnace (RS 120/1000/13), using a heating as well as a cooling rate of 200 K/h.

The charged samples were cleaned with distilled water and isopropanol and then inserted into the TDS chamber. The vacuum pump is initiated, and after 1 hour, the vacuum level is low enough ($<0.35 \times 10^{-3}$ Pa) to be able to start the test. Similar to our previous study,[18] the activation energy was determined by performing TDS tests using four different heating rates, namely 3.33, 6.66, 13.33, and 20 K/min. Subsequently, a deconvolution was applied, and the Lee and Lee[19–21] method was used to correlate peak temperatures with activation energies. Equation [1] is a simplification of the original formula of Kissinger (Eq. [2])[22]:

$$\frac{d\ln(\varphi/T_{\max}^2)}{d(1/T_{\max})} = -\frac{E_A}{R} \qquad [1]$$

$$\frac{\mathrm{d}X}{\mathrm{d}t} = A \cdot (1 - X) \cdot \exp\left(-\frac{E_A}{RT}\right), \qquad [2]$$

where φ is the heating rate (K/s), $T_{\max}$ (K) the TDS peak temperature, E_A (J/mol) is the activation energy for hydrogen desorption of the specific trap associated with $T_{\max}$, R (J/K/mol) is the universal gas constant, X is the released hydrogen fraction, t is the time (min), and A is a frequency factor (s^{-1}).

III. MICROSTRUCTURAL EVALUATION

Figure 2 shows the optical micrographs of the five materials. Due to the lower temperature [1073 K

(800 °C)] used in the heat treatment of C080-H$_2$, grain growth in this material was limited. In the C081-H$_2$ material; the temperature [1173 K (900 °C)] of the heat treatment was significantly higher, and as a result, a grain growth was clearly observed.

IV. HYDROGEN-TRAPPING CAPACITY OF NbC PRECIPITATES

The STEM images and precipitate size distribution of the different C080 alloys are shown in Figure 3. The size distribution of the precipitates present in the C080-HT1 material is uniform with an average size of around 10 nm. Similar precipitates seem to be present in the C080-HT2 material. However, next to these smaller precipitates, of about 15 nm in size, larger-sized precipitates ranging from 100 to 200 nm are also present, leading to a bimodal precipitate size distribution. Different sizes were also observed in the C080-H$_2$ material, in which small (5 nm), medium (30 to 100 nm), and larger precipitates of several hundreds of nanometers are observed. The compositions of these NbC precipitates were confirmed using EDX.

Different samples of the C080-HT1 and C080-HT2 materials were cathodically charged before performing TDS measurements at different heating rates. For the C080-H$_2$ material, cathodic charging was not required as it was already charged during the heat-treatment process in gaseous H$_2$ atmosphere. After the TDS measurements, the resulting peaks are deconvoluted into several individual peaks, as can be seen in Figure 4, which can be attributed to the different traps and are used to calculate the activation energies for desorption from these traps, which are summarized in Table III.

The TDS measurement of C080-HT1 was deconvoluted in two distinct peaks, which resulted in activation energies of 24 and 42 kJ/mol, respectively. The hydrogen desorption giving rise to the first peak is believed to be attributed to hydrogen trapped at grain boundaries. This value is well within the known range of desorption energies for grain boundaries, ranging from 18 to 59 kJ/mol.[5,23,24] Hydrogen trapping at dislocations is more

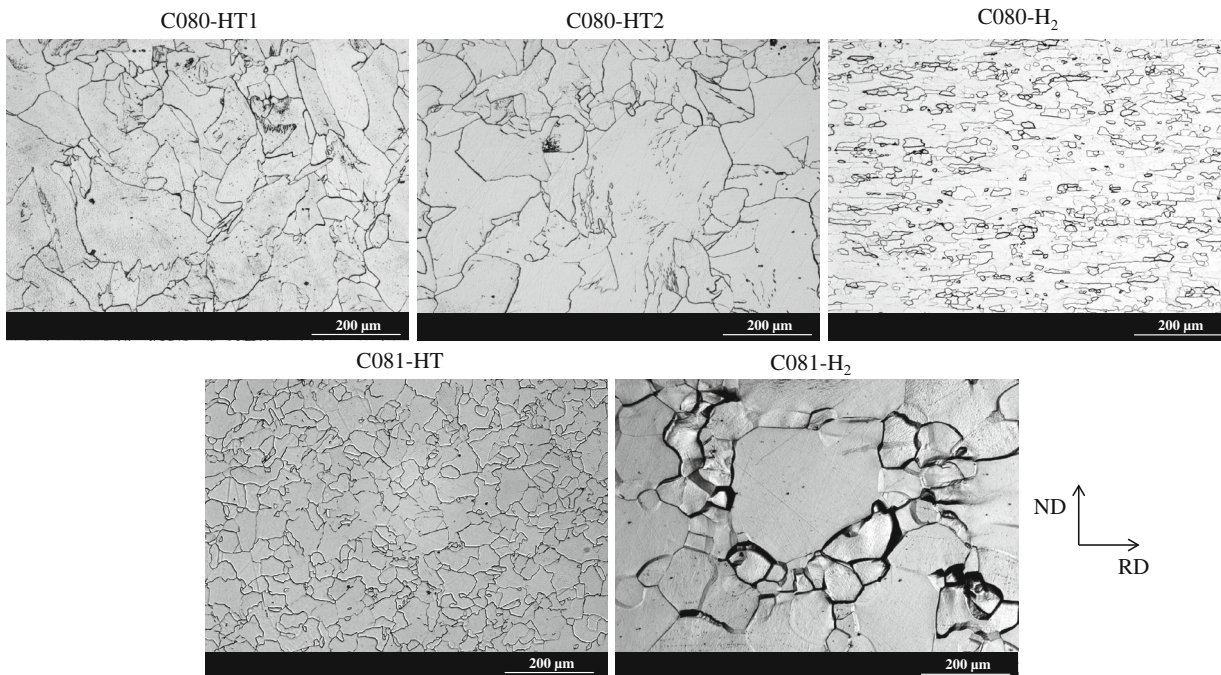C080-HT1   C080-HT2   C080-H$_2$

C081-HT   C081-H$_2$

ND
RD

Fig. 2—Optical microscope pictures of the different materials: *ND*, normal direction; *RD*, rolling direction.

unlikely in the present case, because diffusible hydrogen desorbs from the dislocations before the start of the TDS measurement, as was demonstrated by Pérez Escobar *et al.*[25] The latter peak has slightly higher activation energy and is assumed to be produced by the hydrogen trapped at the small NbC precipitates. The obtained value is well within the range of energies (from 28 to 56 kJ/mol) for nanosized NbC precipitates, as was found by Wei *et al.*[14] As was argued by the group of Tzusaki, the hydrogen is trapped in the core of the misfit dislocations surrounding the broad interface of the small NbC precipitates.[11,14,15]

The deconvolution of the TDS measurement for the C080-HT2 material resulted in three peaks with activation energies of respectively 33, 39, and 48 kJ/mol. The first peak could again be correlated with hydrogen desorption from grain boundaries. The corresponding activation energy is similar to the one obtained for the C080-HT1 material. Since C080-HT1 and C080-HT2 have comparable grain sizes (77 and 69 μm, respectively), the amounts of hydrogen, to which the first peak of the TDS measurement for both materials correlates with, are nearly the same, 1.13×10^{-2} and 0.95×10^{-2} wppm, respectively. The two last peaks are probably due to the hydrogen trapped at the NbC precipitates which are also present in the C080-HT1 material. The appearance of the two peaks which are attributed to one type of trap was already observed by Wei and Tsuzaki[11] for TiC precipitates. This can be explained by the loss of phase boundary coherency with the increasing precipitate size. Consequently, an increase in incoherency and an increase in the corresponding activation energy are expected. The higher activation energy of 48 kJ/mol for the larger precipitates confirms this statement.

The TDS spectra of gaseous charged C080-H$_2$ samples do not show low-temperature peaks, since gaseous charging was performed at temperatures significantly higher than the typical temperature at which the low-temperature peaks occur. Cathodic charging, which generates the low-temperature peak, was not applied after gaseous charging on this material. As such, no desorption energy, for the hydrogen that was trapped in the grain boundaries, could be calculated. A high-temperature peak can be clearly observed. This peak is deconvoluted into two peaks, and calculation of the desorption energies gave their values as 63 and 68 kJ/mol. The interaction of hydrogen with these precipitates might be similar to that for TiC precipitates.[10,11] Hydrogen is considered to be trapped inside the carbon vacancies present in the incoherent NbC precipitates. Gaseous charging at elevated temperatures is required to supply the necessary energy for the hydrogen to enter this hydrogen trap which is not filled by cathodic charging. It is assumed that the two different desorption peaks can be attributed to the bimodal size distribution of the precipitates that tends to be present in the material.

To confirm the hypothesis presented above, an extra TDS measurement was performed on a C080-H$_2$ sample which was, next to gaseous charged, also cathodically charged before the measurement—this sample is called C080-H$_2$EC. This resulted, as expected, in a curve showing two distinct peaks, a low-temperature peak and a high-temperature peak (Figure 4(d)). The low-temperature peak was again attributed to the hydrogen that was introduced by electrochemical charging and trapped at grain boundaries, and at the interface of the smaller precipitates. This peak appears to be much higher than the low-temperature peaks that are observed in the
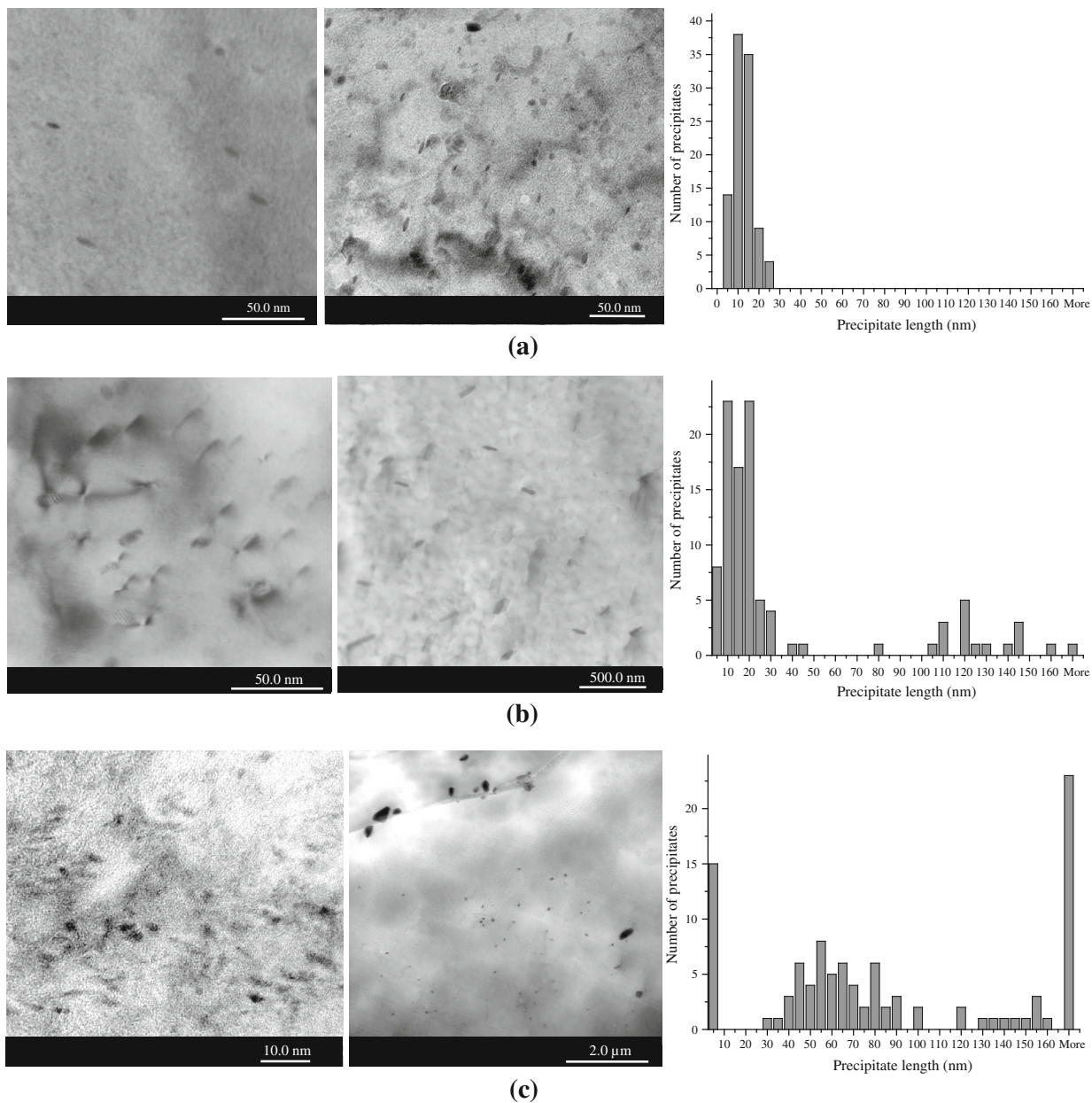
Fig. 3—Bright-field STEM image and size distributions of NbC precipitates in C080-HT1 (*a*), C080-HT2 (*b*), and C080-H₂ (*c*).

C080-HT1 and C080-HT2 materials. This confirms the statement that the hydrogen originating from grain boundaries is the major contribution to this peak, since the C080-H₂ material has a much lower grain size (23 μm), and as such more grain boundaries in which hydrogen is trapped. The amount of hydrogen trapped at the grain boundaries in this material, 1.37×10^{-1} wppm, is also much larger than those for the C080-HT1 and C080-HT2 materials. The shoulder that is formed due to the peak of the small precipitates is significantly reduced compared with the shoulders present in the TDS measurements of C080-HT1 and C080-HT2. Since there are much less small precipitates present in the C080-H₂ material, this is a confirmation that these smaller peaks, present in the TDS spectra of C080-HT1 and C080-HT2, are indeed due to the

hydrogen that is trapped at these precipitates. The high-temperature peak was again attributed to the hydrogen that is introduced by gaseous charging and trapped inside the vacancies of the NbC precipitates.

V. HYDROGEN-TRAPPING CAPACITY OF NbN PRECIPITATES

The STEM images and precipitate size distributions of the different C081 alloys are shown in Figure 5. The C081-HT material has a wide range of smaller sized precipitates between 5 and 100 nm, next to the larger cuboid precipitates of over 100 nm. The C081-H₂ material does not contain very small precipitates, but has a wide range of precipitates larger than 50 nm.
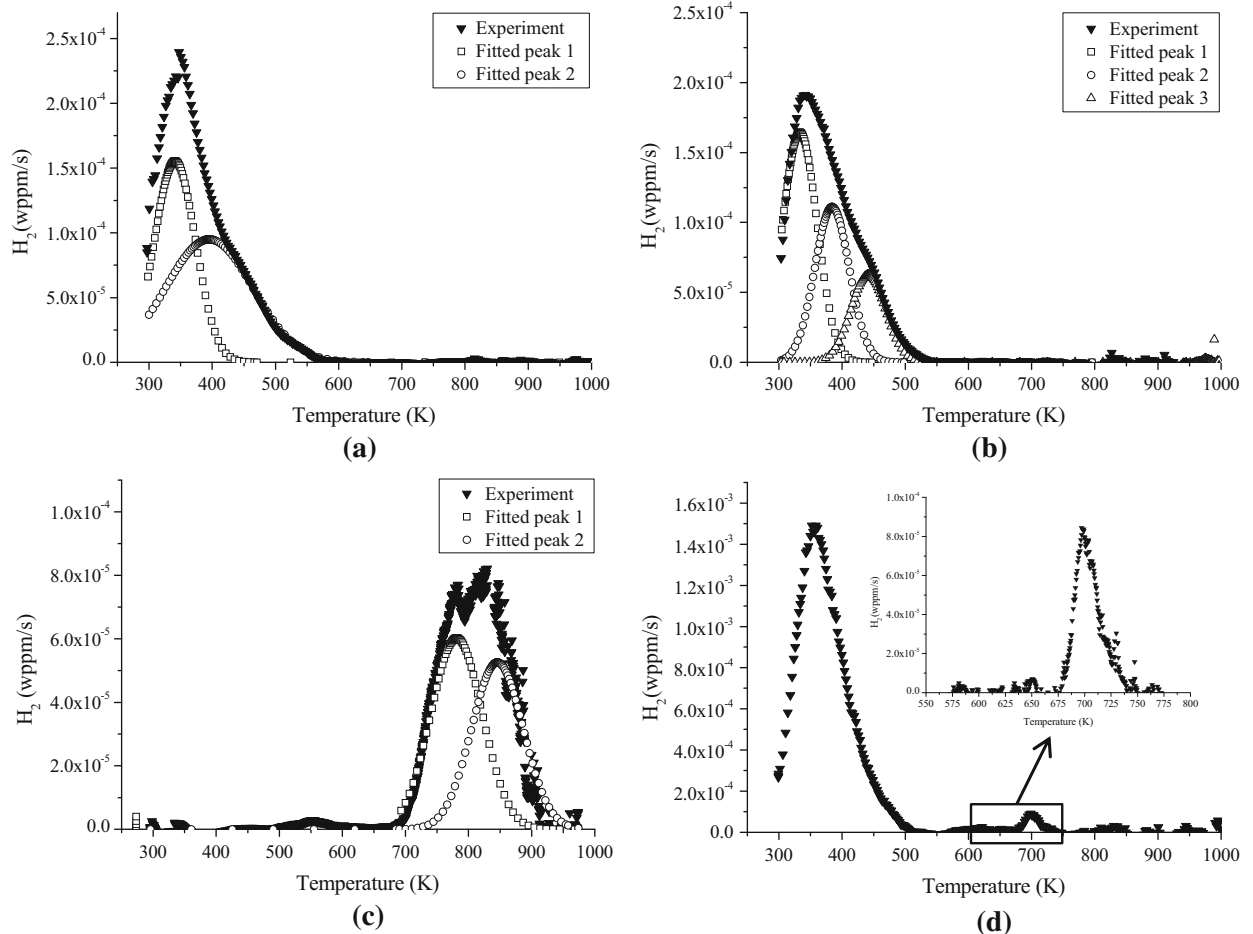
Fig. 4—TDS spectra of C080-HT1 (*a*) and C080-HT2 (*b*) after electrochemical charging, C080-H$_2$ (*c*) after gaseous charging, and C080-H$_2$EC (*d*), after both electrochemical and gaseous chargings; heating rate 6.66 K/min.

Table III. Calculated Activation Energies for the Deconvoluted Peaks of the Materials C080-HT1, C080-HT2, and C080-H$_2$

Material	E_A Peak 1 (kJ/mol)	E_A Peak 2 (kJ/mol)	E_A Peak 3 (kJ/mol)
C080-HT1*	24 ± 1	42 ± 9	—
C080-HT2	33 ± 1	39 ± 2	48 ± 1
C080-H$_2$	63 ± 4	68 ± 5	—

*Activation energies calculated using only three heating rates, due to failure of the measurement with heating rate of 20 K/min.

After deconvolution, the TDS spectra of the C081-HT material show the three distinct peaks that can be seen in Figure 6. Their calculated hydrogen activation energies for desorption are 27, 23, and 24 kJ/mol, respectively (Table IV). The first and the largest peak can again be attributed to desorption of hydrogen for the grain boundaries, as was also observed for the C080 material. Again, the peak makes up the largest part of the total hydrogen desorption. Using the area underneath the peak, the amount of hydrogen that is associated with this peak is 1.40×10^{-2} wppm. This is slightly more than for the C080-HT1 (77 μm) and C080-HT2 (69 μm) material, which is due to the smaller grain size of the C081-HT material (33 μm). The latter two peaks show similar activation energies, which are assumed to be produced by

the hydrogen trapped in the misfit dislocations at the NbN precipitates. The last peak shows a larger standard deviation; this could be due to the large range of precipitate sizes, giving also a range in activation energies. The last two peaks appear to have lower activation energies compared with the first peak; however, hydrogen is released at slightly higher temperatures. This was also observed in previous studies of Pérez Escobar[10] and Tsuzaki and co-workers,[11] who found a number of peaks with similar energies. This can be explained by the parameter A, the frequency factor in the Kissinger equation (Eq. [2]), of the different peaks, which decreased with the increasing peak temperature. This parameter represents the probability per unit of time of successful desorption of a hydrogen atom from a trap.
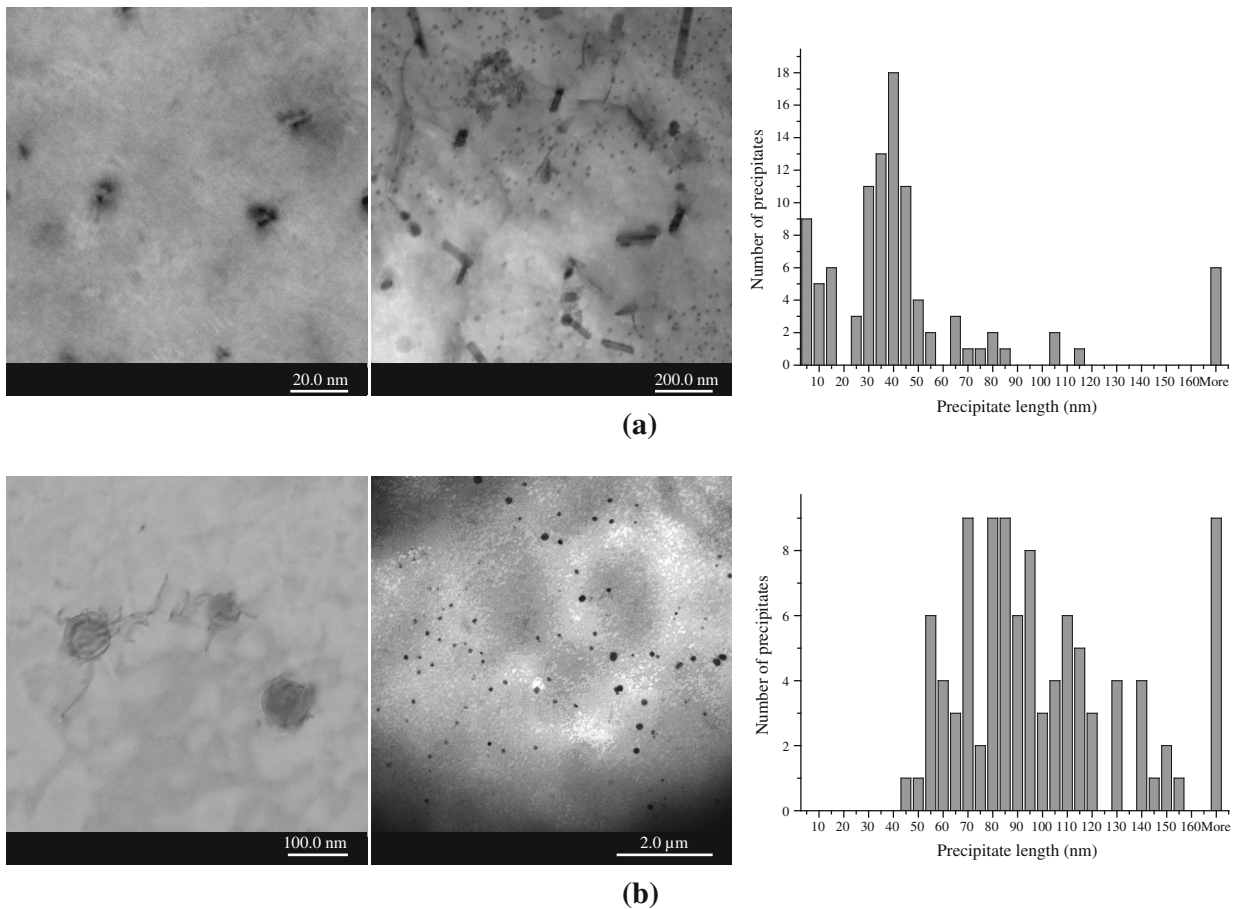
(a)

(b)

Fig. 5—Bright-field STEM images and size distributions of NbN precipitates in C081-HT (*a*) and C081-H$_2$ (*b*).

The TDS spectra of C081-H$_2$ were deconvoluted into only two peaks as shown in Figure 6. These peaks appear to be originating from hydrogen with an activation energy for desorption ranging between 100 and 143 kJ/mol (Table IV). These values appear to be significantly higher than the activation energies of NbC precipitates. However, this energy range has also been observed for TiC precipitates which were charged under similar condition by Pérez Escobar *et al.*[10]

Again, a TDS measurement was performed of a C081-H$_2$ sample that was also electrochemically charged before the measurement, and this sample is called C081-H$_2$EC. Two distinct peaks appear in the spectrum, a low-temperature and a high-temperature peak. The low-temperature peak is due to the hydrogen released from grain boundaries. Due to the larger grain size of this material (56 μm), the amount of hydrogen that is associated with this peak (1.22 × 10^{-2} wppm) is lower than for the C081-HT material. Since there are no small precipitates present inside this material, no shoulder appears on this peak, as is the case for the C081-HT material. This proves that the peaks in TDS spectrum of C081-HT were attributed in the right way. The high-temperature peak is caused by the desorption of H$_2$ from the large incoherent precipitates, and this is similar to that for C081-H$_2$.

VI. CONCLUSIONS

TDS measurements were performed on lab-cast materials containing NbC or NbN precipitates. By applying different heat treatments, materials with different precipitate size distributions were obtained. Cathodic charging gave rise to a low-temperature peak [323 K to 523 K (50 °C to 250 °C)], originating from the hydrogen trapped near grain boundaries, with activation energy ranging between 24 and 33 kJ/mol, and at the interface of small precipitates, from 23 to 48 kJ/mol. Charging in the gaseous environment gave rise to a high-temperature TDS peak [723 K to 923 K (450 °C to 650 °C)], which was attributed to the presence of incoherent precipitates, the activation energy for NbC precipitates ranged between 63 and 68 kJ/mol and for NbN precipitates, and this appeared to be somewhat higher, ranging between 100 and 143 kJ/mol. Gaseous charging at elevated temperature is considered to be an absolute prerequisite to provide the required energy to trap hydrogen in the vacancies of the precipitates. This trap was different from the one charged by electrochemical charging. Moreover, when an extra electrochemical charging was performed on the gaseous-charged materials, an additional low-temperature peak occurred in the TDS spectrum next to the high-temperature peak. In this low-temperature peak, a strongly reduced shoulder
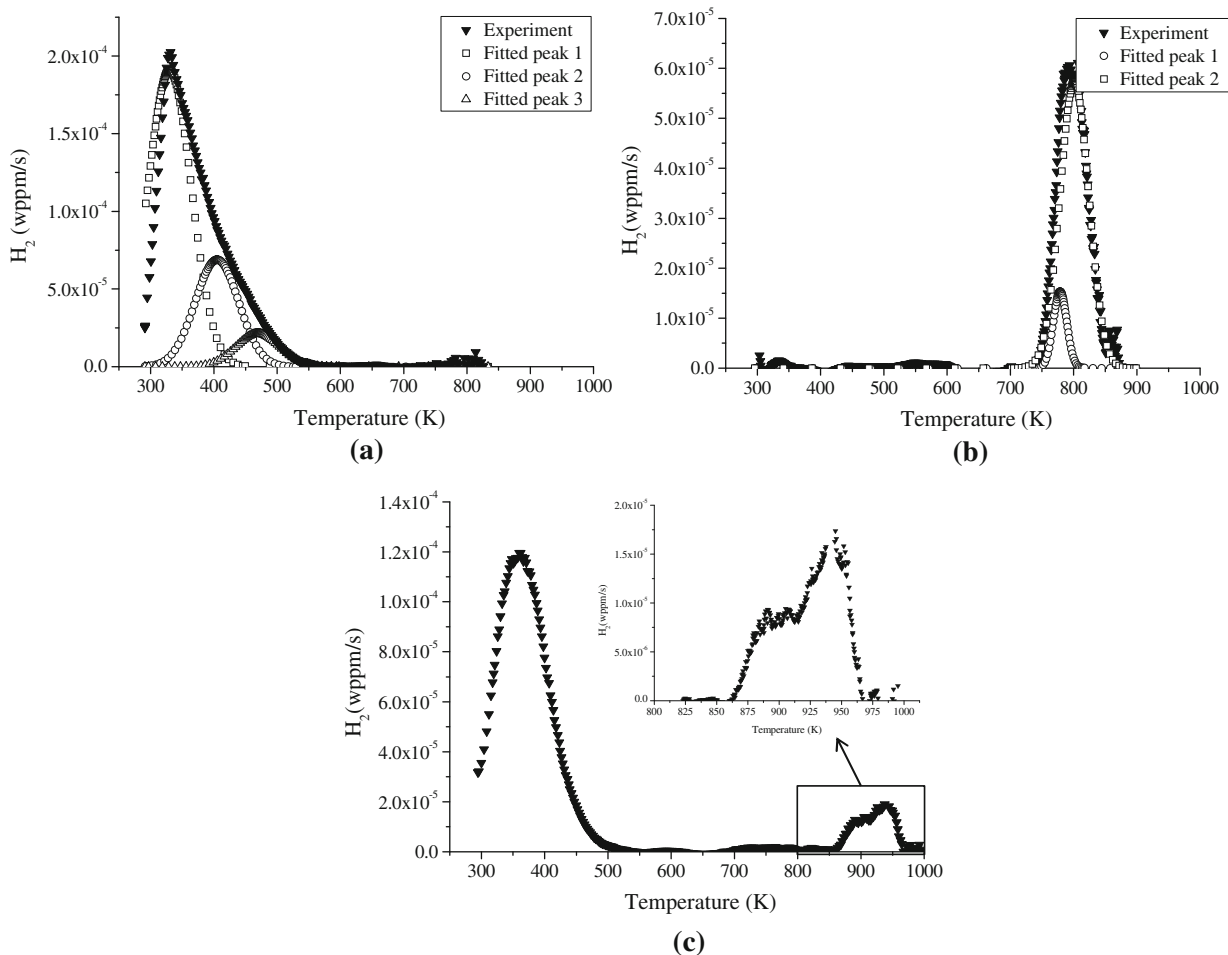
Fig. 6—TDS spectra of C081-HT (*a*) after electrochemical charging; C081-H$_2$ (*b*) after gaseous charging; and C081-H$_2$EC (*c*) after both electrochemical and gaseous charging; heating rate 6.66 K/min.

Table IV. Calculated Activation Energies for the Deconvoluted Peaks of the Materials C081-HT and C081-H$_2$

Material	E_A Peak 1 (kJ/mol)	E_A Peak 2 (kJ/mol)	E_A Peak 3 (kJ/mol)
C081-HT	27 ± 3	23 ± 4	24 ± 13
C081-H$_2$	143 ± 17	100 ± 34	—

appeared, since much less small precipitates were present in the material produced by the low-temperature heat treatment during gaseous charging.

REFERENCES

1. L. Duprez, K. Verbeken, and M. Verhaege: *Proc. 2008 Int. Hydrogen Conf.*, 1st ed., ASM International, Wyoming, WY, 2008, pp. 62–69.
2. T. Depover, D. Pérez Escobar, E. Wallaert, Z. Zermout, and K. Verbeken: *Int. J. Hydrogen Energy*, 2014, DOI:10.1016/j.ijhydene.2013.12.190.
3. H. Asahi, D. Hirakami, and S. Yamasaki: *ISIJ Int.*, 2003, vol. 43, pp. 527–33.
4. B. Malard, B. Remy, C. Scott, A. Deschamps, J. Chene, T. Dieudonne, and M.H. Mathon: *Mater. Sci. Eng. A*, 2012, vol. 536, pp. 110–16.
5. T. Asaoka, G. Lapasset, M. Aucouturier, and P. Lacombe: *Corros. NACE*, 1978, vol. 34, pp. 39–47.

6. G.M. Pressouyre and I.M. Bernstein: *Metall. Trans. A*, 1978, vol. 9A, pp. 1571–80.
7. M.A.V. Devanathan and Z. Stachurski: *Proc. R. Soc. Lond. Ser. A*, 1962, vol. 270, pp. 90–102.
8. H.G. Lee and J.Y. Lee: *Acta Metall.*, 1984, vol. 32, pp. 131–36.
9. F.G. Wei, T. Hara, and K. Tsuzaki: *Metall. Mater. Trans. B*, 2004, vol. 35B, pp. 587–97.
10. D. Pérez Escobar, E. Wallaert, L. Duprez, A. Atrens, and K. Verbeken: *Met. Mater. Int.*, 2013, vol. 19, pp. 741–48.
11. F.G. Wei and K. Tsuzaki: *Metall. Mater. Trans. A*, 2006, vol. 37A, pp. 331–53.
12. J. Takahashi, K. Kawakami, Y. Kobayashi, and T. Tarui: *Scripta Mater.*, 2010, vol. 63, pp. 261–64.
13. M. Ohnuma, J.I. Suzuki, F.G. Wei, and K. Tsuzaki: *Scripta Mater.*, 2008, vol. 58, pp. 142–45.
14. F. Wei and K. Tsuzaki: *Proc. 2008 Int. Hydrogen Conf.*, 1st ed., ASM International, Wyoming, WY, 2008, pp. 456–63.
15. F. Wei, T. Hara, and K. Tsuzaki: *Proc. 2008 Int. Hydrogen Conf.*, 1st ed., ASM International, Wyoming, WY, 2008, pp. 448–55.
16. D. Pérez Escobar, L. Miñambres, L. Duprez, K. Verbeken, and M. Verhaege: *Corros. Sci.*, 2011, vol. 53, pp. 3166–76.
17. D. Pérez Escobar, L. Duprez, A. Atrens, and K. Verbeken: *J. Nucl. Mater.*, 2014, DOI:10.1016/j.jnucmat.2013.07.006.
18. D. Pérez Escobar, L. Duprez, K. Verbeken, and M. Verhaege: *Mater. Sci. Eng. A*, 2012, vol. 551, pp. 50–58.
19. S. Lee and J. Lee: *Metall. Trans. A*, 1986, vol. 17A, pp. 181–87.
20. J.Y. Lee and S.M. Lee: *Surf. Coat. Technol.*, 1986, vol. 28, pp. 301–14.
21. J. Lee and J. Lee: *Met. Sci.*, 1983, vol. 17, pp. 426–32.
22. H.E. Kissinger: *Anal. Chem.*, 1957, vol. 29, pp. 1702–06.
23. W. Choo and J. Lee: *Metall. Trans. A*, 1982, vol. 13A, pp. 135–40.
24. A. Kumnick and H. Jonhson: *Acta Metall.*, 1980, vol. 28, pp. 33–39.
25. D. Pérez Escobar, T. Depover, L. Duprez, K. Verbeken, and M. Verhaege: *Acta Mater.*, 2012, vol. 60, pp. 2593–2605.